Intrinsic resonant photoionization time delay of hydrogen atoms probed with attosecond beating of asymmetrical photon transitions

Xiaoyang Yu,[1] Meng Han,[1,2] Zhenning Guo,[1] and Yunquan Liu[1,3,4]

[1]*State Key Laboratory for Mesoscopic Physics and Collaborative Innovation Center of Quantum Matter, School of Physics, Peking University, Beijing 100871, China*

[2]*Laboratorium für Physikalische Chemie, ETH Zürich, Zürich 8093, Switzerland*

[3]*Center for Applied Physics and Technology, HEDPS, Peking University, Beijing 100871, China*

[4]*Collaborative Innovation Center of Extreme Optics, Shanxi University, Taiyuan, Shanxi 030006, China*

(Received 16 August 2021; accepted 30 November 2021; published 10 December 2021)

We investigate the benchmark photoionization of hydrogen atoms triggered by the third harmonic at vacuum ultraviolet laser pulses (at 202 nm) and probe the time delay via resonant quantum states with the weak fundamental laser pulses (at 606 nm). As a result, two different sidebands will emerge below the first above threshold ionization peak. We show that these two sidebands can be established through resonance with the $3d$ and $2p$ states of hydrogen atoms at 202 nm, respectively. Using this scheme, we can extract the angularly dependent time delay of electrons liberated from the $3d$ state with respect to those released from the $2p$ state by comparing the phase differences between two sidebands. Using the attosecond beating scheme of asymmetrical photon transition, we obtain the intrinsic time delay between the $3d$ and $2p$ excited electronic states in the few-photon ionization regime of H atoms, which is $\sim$103 as. This asymmetric attosecond beating metrology provides insight into electron dynamics of the multiphoton resonant ionization via multi-intermediate states.

DOI: 10.1103/PhysRevA.104.063108

I. INTRODUCTION

With the development of attosecond light pulses, it becomes a routine approach to probe the intra-atomic electron dynamics in photoionization from atoms [1,2], molecules [3], to solids [4,5]. Generally, electron dynamics can be revealed by the attosecond streaking camera [6–8], the reconstruction of attosecond beating by interference of two-photon transition (RABBITT) [9,10], attosecond angular streaking by elliptically (circularly) polarized fields or bicircular fields [11–14]. The RABBITT measurement consists of a pump pulse of extreme ultraviolet (XUV) attosecond pulse train from high-order harmonic generation and a probe pulse of the weak fundamental infrared (IR) laser field [15–17]. The measurement has high spectral resolution and thus becomes an indispensable tool for attosecond chronoscopy [18]. The XUV laser pulses can excite the electron to resonant states [8,19–22] to derive the time delay near the threshold [23–26]. Very recently, the angle-dependent He and Ne resonant RABBITT measurement was proposed [27]. The probing process of RABBITT is based on the interference of two-photon (XUV+IR) transition channels, which are inevitably involved with the phase of the continuum-continuum transition in the presence of the long-range Coulomb potential [28,29], and the Wigner scattering phase that is determined by the energy and the angular momenta of the initial and the final states [30–33]. The RABBITT can be used in the multiphoton ionization regime [34,35]. In typical RABBITT measurement, there is only one SB in the adjacent main peaks. The observation quantity causes difficulty disentangling them and obtaining the angle dependent Wigner time delay [36–38], or continuum-continuum transition phase [39,40]. Thus, these two phases are entangled in the observation quantity, i.e., the oscillation phase of the sideband (SB). The improvement of the RABBITT technique with multi-SBs will be necessary. Very recently, the twin sidebands scheme was used for the temporal characterization of the shaped free-electron laser pulse [41].

In this paper, we study the interference of asymmetrical-photon transition across the ionization threshold of hydrogen atoms to probe the intrinsic time delay between the formations of electron wave packets originating from different atomic subshells. With a weak fundamental laser pulse and its third harmonic, the twin different SBs emerge below the first above-threshold ionization (ATI). These two SBs are formed by the channel interference between the first ATI and $3d$ and $2p$ bound state by using the specific wavelength at 202 nm. By changing the relative phase between two-color laser pulses, one can resolve the angular-dependent phase difference of two SBs. Considering the continuum-continuum transition time delay from the first ATI to two SBs and the short Coulomb potential scattering time delay from direct ionization of different atomic subshells, we can derive the time delay between the $3d$ state and $2p$ state by comparing the phase difference between two SBs. Alternatively, we have also tracked the evolution trajectories of $3d$ and $2p$ partial waves in single VUV laser pulse to obtain the time delay between the two different subshells. It is shown that the asymmetrical-photon transition approach can probe the subcycle angular-dependent multiphoton ionization dynamics in attosecond time scale.

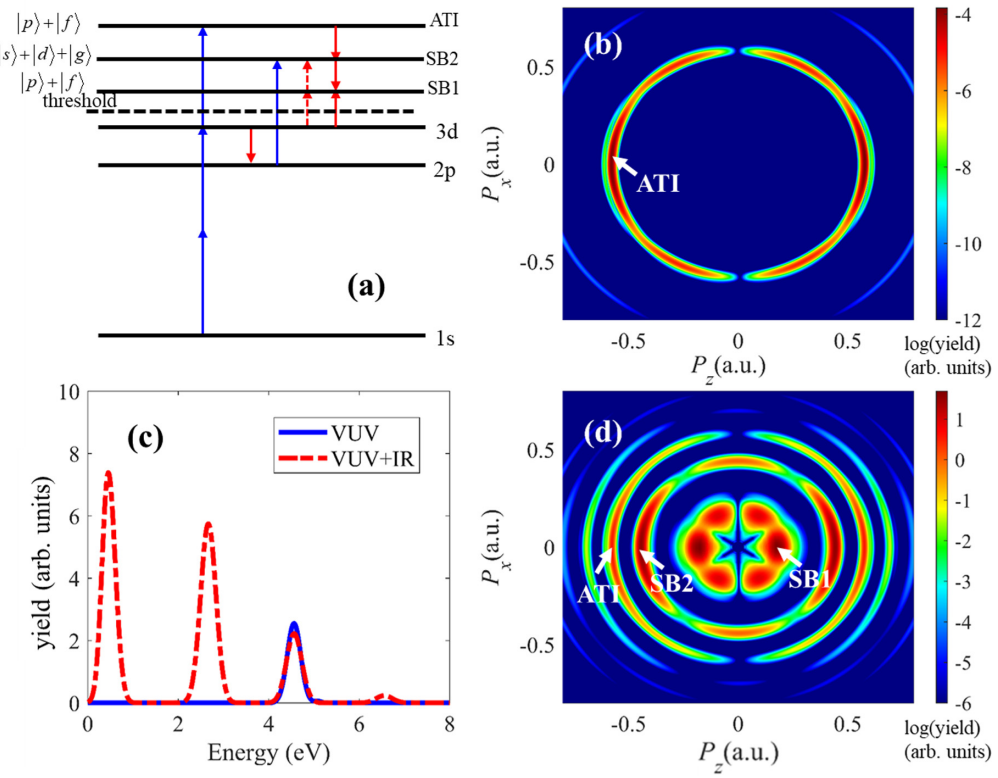

FIG. 1. (a) The involved energy level of bound states and continuum states for hydrogen atom. The dashed line is the ionization threshold. (b) The photoelectron momentum distribution of hydrogen atom in single VUV laser pulse at ∼202 nm. (c) The corresponding energy spectrum of photoelectron in single VUV (blue line) and two-color laser pulses (red dashed line). (d) The photoelectron momentum distribution of hydrogen atom in two-color laser pulse with the integration of the relative phase between two-color laser pulses.

II. METHOD

We numerically solve the three-dimensional time-dependent Schrödinger equation (TDSE), which is given by

$$i\frac{\partial}{\partial t}\varphi(\mathbf{r},t)=\left(-\frac{\nabla^2}{2}+V(\mathbf{r})+\mathbf{r}\cdot\mathbf{E}\right)\varphi(\mathbf{r},t), \tag{1}$$

where $V(\mathbf{r})=-1/r$ is the Coulomb potential [atomic units (a.u.) are used throughout this paper unless stated otherwise]. The electric field $\mathbf{E}$ is

$$\mathbf{E}=E_{\text{fundamental}}f_1(t)\cos(\omega t)\mathbf{e}_z+E_{\text{VUV}}f_1(t)\cos(3\omega t+\varphi)\mathbf{e}_z, \tag{2}$$

where E_{VUV} is the amplitude of the vacuum ultraviolet (VUV) laser field, and $E_{\text{fundamental}}$ is the amplitude of the fundamental laser field. Both fields are polarized along the z axis. ω is the frequency of the fundamental laser field, and φ is the relative phase between the fundamental laser field and the VUV laser field. $f_1(t)$ is the envelope of the laser field. Both the laser pulses are sine-square envelopes with the pulse duration of ten periods of the fundamental laser field. In the calculation, the ionization pulse is the third harmonic with the peak intensity of 2×10^{13} W/cm^2 at a wavelength of 202 nm. The intensity of the probing field is 1×10^{12} W/cm^2 at the wavelength of 606 nm.

III. RESULTS AND DISCUSSION

Different from traditional RABBIITT (symmetrical-photon transition), attosecond beating of asymmetrical-photon transition is a new scheme to probe the photoelectron time delay, which have two SBs in adjacent ATI peaks. The number of releasing photons from the higher ATI is different from the number of absorbing photon from the lower ATI. The sketch of the asymmetrical-photon transition across the ionization threshold with related energy level of the bound state for hydrogen atom is shown in Fig. 1(a). The ionization threshold is marked as the dashed line. The energy gap between the $3d$ state and the $1s$ ground state is about twice the one photon energy of the vacuum ultraviolet laser pulse. After adding the fundamental laser pulse, the electrons can be pumped from the $3d$ state to the $2p$ state. Therefore, two emerging SBs are associated with the atomic bound state $3d$ and $2p$ via the asymmetrical-photon transition, respectively. In the third harmonic field solely, the photoelectron momentum distribution is illustrated in Fig. 1(b). If introducing the weak fundamental laser field, two SBs emerge below the first ATI peaks, as shown in the phase-integrated photoelectron momentum distribution [Fig. 1(d)]. The energy spectrum of the first ATI peak (blue solid line) is formed with the three-photon ionization from the ground state $1s$, as displayed in Fig. 1(c).The yields of two SBs (red dashed line) are larger than the first ATI.

In the specific geometry, these two SBs mainly originate from the interference between the asymmetrical transition

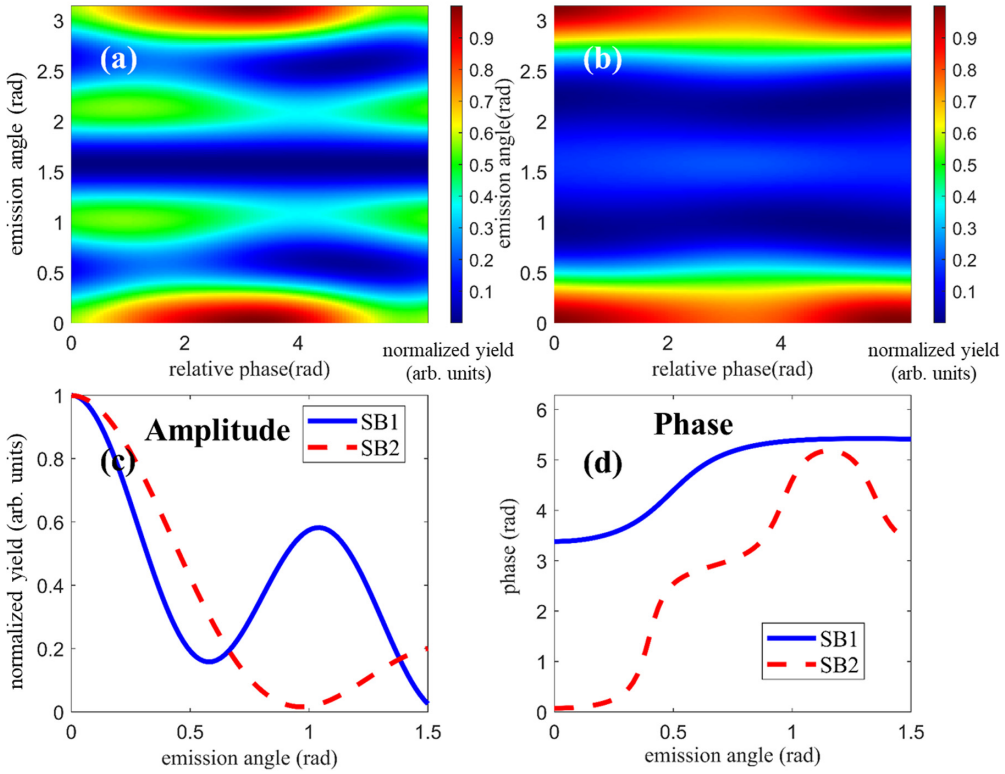

FIG. 2. The phase-resolved and angular-resolved photoelectron momentum distribution of SB1 (a) and SB2 (b), respectively. The amplitude (c) and phase (d) calculated from the Fourier transform of the phase-resolved and angular-resolved photoelectron momentum distribution of SB1 and SB2, respectively.

paths from the first ATI and different discrete states ($3d$ state and $2p$ state). The lower SB (SB1) is formed by the interference between the channels of absorbing one fundamental photon from the $3d$ bound state and releasing two fundamental photons from the first ATI. Similar to SB1, the higher SB (SB2) is formed by the interference between the channels of absorbing one VUV photon from the $2p$ bound state and releasing one fundamental photon from ATI. According to the selection rule, the final state of SB1 is composed of the quantum state with the orbital quantum number $l = 1$ or $l = 3$ and the final state of SB2 is composed of the quantum states of the orbital quantum number $l = 0$, $l = 2$ or $l = 4$. Note that there is another transition path via absorbing two fundamental photons via the $3d$ state that can contribute to the SB2, as shown in red dashed arrows in Fig. 1(a). Because the probing laser field is very weak, this two photon transition probability would be much weaker than that of the $2p$ state with one 202-nm photon involved.

In traditional RABBIT experiments, the phase shift of the SB with respect to its nearby photoelectron peaks from the subsequent high harmonic photon is about π. The interesting question would be what the phase difference between SB1 and SB2 is, and what we can learn from the phase difference for the asymmetrical photon transition. We show the phase-resolved and angular-resolved photoelectron momentum distribution of SB1 and SB2 in Figs. 2(a) and 2(b), respectively. It is obvious that two SBs oscillate with different phases and both of them have a strong dependence on the electric emission angle. The oscillation of the SB yields can be expressed as

$$S(\tau) = \alpha(\theta) + \beta(\theta)\cos\left[3\omega\tau + \varphi_R(\theta)\right], \tag{3}$$

where α and β are the angular-dependent amplitudes which depend on the weight of each transition channel, $\varphi_R(\theta)$ is the phase difference between the neighboring ATIs, and τ is the relative time delay between the VUV and the fundamental laser pulses. As seen the field envelope in the Eq. (2), when the laser pulses changes one cycle of the VUV laser pulse, the relative phase φ changes from 0 to 2π. Therefore, the yield of SBs oscillates with the driving laser frequency 3ω.

We can further obtain the normalized amplitude and the phase of two SBs by performing the Fourier transform of the time-resolved and angular-resolved photoelectron momentum distribution of SB1 and SB2, as shown in Figs. 2(c) and 2(d), respectively. According to the selection rule, one can find that the SB1 (blue line) consists of p partial wave and f partial wave. The SB2 (red dashed line) consists of d partial wave, s partial wave, and g partial wave. The angular-resolved phase of SB1 (blue curve) changes sharply when the amplitude ratio of different partial waves changes inversely, where the emission angle is around 0.5 rad. The angular-resolved phase of SB2 (red dashed line) is more complex because of high order partial wave (g state) through the transition channel absorbing two photons of fundamental laser pulse from $3d$.

In order to understand the phase differences of the SBs in this asymmetrical transition geometry, the angular-dependent

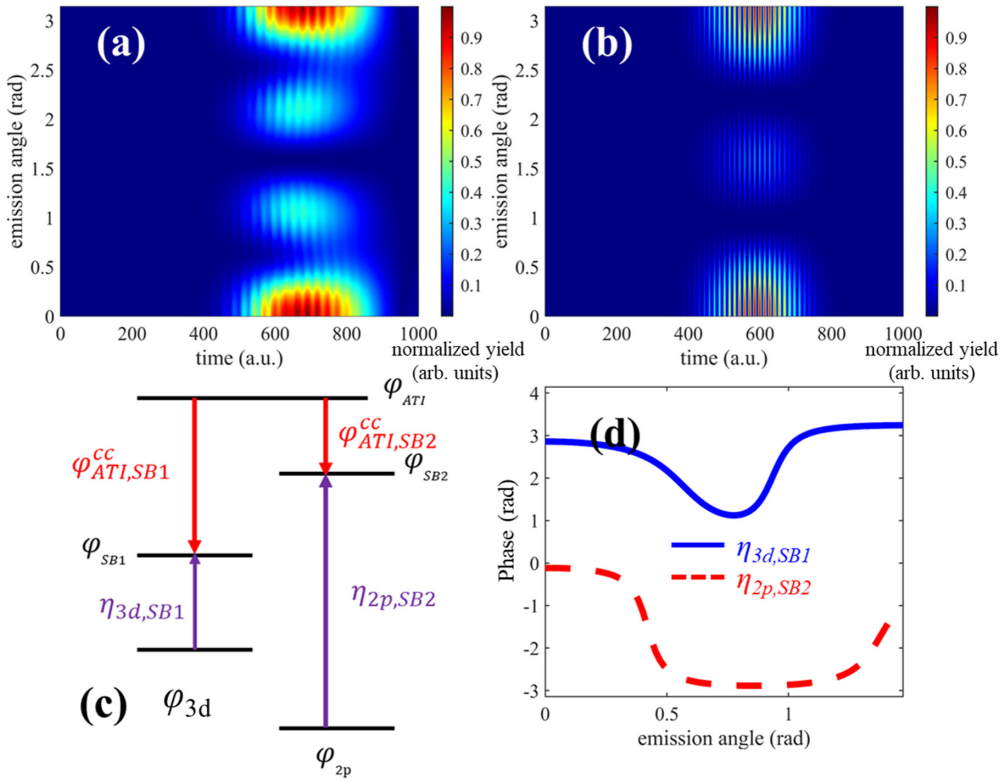

FIG. 3. The angular-resolved of time-resolved photoelectron momentum distribution calculated on solving time dependent Schrödinger equation with the partial wave expansion of $3d$ (a) and $2p$ (b), respectively. (c) The sketch of the source of phases in different interference channels for SBs. (d) The angular-resolved scattering phase from two bound-continuum transition channels from $3d$ (blue line) and $2p$ (red dashed line) state, calculated on Fourier transform of (a) and (b), respectively.

phase of two SBs in Fig. 3(c) can be decomposed as

$$\varphi_{\mathrm{SB1}}(\theta) = \varphi_{\mathrm{ATI}}(\theta) + \varphi^{cc}_{\mathrm{ATI,SB1}} - \varphi_{3d}(\theta) - \eta_{3d,\mathrm{SB1}}(\theta),$$
$$\varphi_{\mathrm{SB2}}(\theta) = \varphi_{\mathrm{ATI}}(\theta) + \varphi^{cc}_{\mathrm{ATI,SB2}} - \varphi_{2p}(\theta) - \eta_{2p,\mathrm{SB2}}(\theta), \quad (4)$$

where φ_{ATI} is the phase for absorbing three VUV photons from $1s$, and φ^{cc} is the laser-driven transition connecting phase between ATI and SBs in the presence of long-range Coulomb potential. η is the scattering phase shift of the intermediate state and is identical to the phase of the corresponding one-photon ionization [29]. φ_{3d} and φ_{2p} are the intrinsic phases for the intermediate states $3d$ and $2p$, respectively.

The φ_{cc} in Eq. (4) can be analytically derived. φ_{cc} corresponds to the one-photon free-free transition of the photoelectron in the vicinity of the parent ion, which can be expressed [29] as

$$\varphi^{cc}_{k,\kappa} = \arg\left(\frac{(2\kappa)^{iZ/\kappa}}{(2k)^{iZ/k}} \frac{\Gamma[2 + iZ(1/\kappa - 1/k)]}{(\kappa - k)^{iZ(1/\kappa - 1/k)}}\right), \quad (5)$$

where κ is the momentum of the initial state in the continuum, k is the momentum of the final state after the exchange of one fundamental photon, and Z is the remaining charge on the parent ion. Here, based on the asymptotic approximation, one can see that the continuum-continuum transition is independent of the short-range behavior of the atomic potential and therefore universal. Based on Eq. (5), we obtain that the continuum-continuum transition time delay from ATI to SB2 is $\varphi^{cc}_{\mathrm{ATI,SB2}} = 0.78$ rad. The two-photon transition can be divided into two steps. The first step is to release one photon from the ATI to the immediate state. The second step is to release another photon from the immediate state to SB1. The phase shift of two transition steps is obtained from Eq. (5). The continuum-continuum transition time delay from ATI to SB1 is $\varphi^{cc}_{\mathrm{ATI,SB1}} = 2.38$ rad.

The single photon scattering phase η for a hydrogenic system cannot be analytically expressed in the multiphoton ionization regime. Therefore, we obtain the single photon scattering phase by numerically solving the time-dependent Schrödinger equation with partial wave expansion. In our simulation, the wave function is expanded to the basis vector with different partial waves, which correspond to different discrete states. The maximum orbital quantum number is set as 15 to ensure the accuracy of calculation. The total wave function can be expressed as $\varphi_{\mathrm{total}}(t) = \sum_{\mathrm{n,l}} \alpha_{\mathrm{nl}}(t)\varphi_{\mathrm{nl}}(t) = \sum_{\mathrm{n,l}} \alpha_{\mathrm{nl}}(t)\mathrm{R_{nl}(r,t)P_{nl}}(\theta)$, where φ_{nl} is the wave function of the bound state with a certain main quantum number n and orbital quantum number l and α_{nl} is the weight of the wave function. $\mathrm{R_{nl}(r,t)}$ and $\mathrm{P_{nl}}(\theta)$ are the radial and angular wave function, respectively. We define the absorbing boundary $R = 100$ a.u. as the criterion of ionization and collecting the wave function out of the absorbing boundary. The ionized wave function $\varphi_{\mathrm{i}} = \varphi_{\mathrm{total}}Fs$, where Fs is the boundary absorption function. The remaining part of the wave function can be expressed as $\varphi_{\mathrm{re}} = \varphi_{\mathrm{total}} - \varphi_{\mathrm{i}} = (1 - Fs)\varphi_{\mathrm{total}}$. To obtain the photoelectron momentum distribution, the ionized wave function φ_i is projected onto the momentum space. The

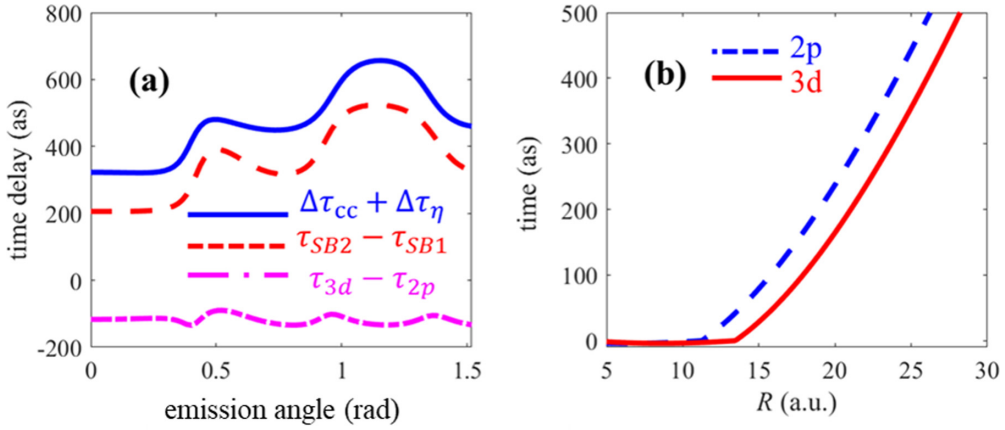

FIG. 4. (a) The angular-resolved time delay between two SBs (red dashed line), the angular-resolved time delay between $3d$ and $2p$ state (purple dot dashed line), the angular-resolved time delay from one-photon continuum-continuum transition and one-photon bound-continuum transition (blue line). (b) The trajectories of wave packet of $3d$ (red line) and $2p$ (blue dashed line) state in single VUV laser pulse.

wave function of continuum states in momentum space can also be expanded to the basis vector with different partial wave $\varphi_{\text{momentum}}(t) = \sum_{\varepsilon,l} \beta_{\varepsilon l}(t)\varphi_{\varepsilon l}(t) = \sum_{\varepsilon,l} \beta_{\varepsilon l}(t)\mathrm{B}_{\varepsilon l}(t)Y_{\varepsilon l}(\theta)\mathrm{e}^{i\eta_{\varepsilon l}}$ where $\varphi_{\varepsilon l}$ is the wave function of the continuum state with a certain energy ε and orbital quantum number l and β_{nl} is the weight of wave function. $Y_{\varepsilon l}(\theta)$ is the spherical harmonics and η is the transition phase. B is the transition amplitude and we define the equivalent transition amplitude $A = \beta \mathrm{B}$ in the calculation.

Then, the φ_{3d} and φ_{2p} can be separated artificially from the total wave function. We propagate the individual wave function to infinity and probe by the virtual detector. We record the time-resolved and the angular-resolved photoelectron momentum distribution by projecting the ionized wave functions $\alpha_{3\mathrm{d}}\varphi_{\mathrm{i,3d}}$ and $\alpha_{2\mathrm{p}}\varphi_{\mathrm{i,2p}}$ onto the momentum space, as shown in Figs. 3(a) and 3(b), respectively. The equivalent transition amplitude A and transition phase η can be obtained by Fourier transform of the time-resolved momentum distribution of $\varphi_{\text{momentum}}$.

To decode the origin of angular-dependent phase difference, the ionized wave functions $\varphi_{\mathrm{i,3d}}$ and $\varphi_{\mathrm{i,2p}}$ are projected onto different wave function $\varphi_{\varepsilon l}$ in the momentum space. For SB1, it is dominated by the f and p partial wave, and the orbital angular momentum quantum numbers are $l = 1$ and $l = 3$, respectively. The bound-free transition phase is given by $\eta_{3d,\mathrm{SB1}} = \arg[A_p Y_p e^{i\eta_p} + A_f Y_f e^{i\eta_f}]$. We can obtain the amplitude ratio of the f partial wave and p partial wave $A_f : A_p = 2.69 : 1$, which represents the yield ratio of two transition channels. And we obtain the phase difference between the f partial wave and p partial wave is $\eta_f - \eta_p = 2.92$ rad. Similar to SB1, SB2 can be decomposed by s, d, and g partial waves. The bound-free transition phase of SB2 is given by $\eta_{2p,\mathrm{SB2}} = \arg[A_s Y_s e^{i\eta_s} + A_d Y_d e^{i\eta_d} + A_g Y_g e^{i\eta_g}]$. We obtain the amplitude ratio of s, d, and g partial waves as $A_s : A_d : A_g = 1.45 : 3.4 : 1$ and the phase of s, d, and g partial waves is η_s, η_d, $\eta_g = 2.63$, 5.08, 3.83 rad. The equivalent angular-resolved scattering phases of two bound-continuum transition channels from the $3d$ (blue line) and $2p$ (red dashed line) states are displayed in Fig. 3(d).

With the above analysis, one can obtain the time delay between two SBs, the continuum-continuum transition time delay from ATI to SBs, and the scattering time delay by bound-continuum transition from the $3d$ and $2p$ states, separately. Note that the phase differences are converted to the corresponding time delays by a finite difference formula $\Delta\tau = \Delta\varphi/3\omega$. From Eq. (4), the time delay between $3d$ and $2p$ can be expressed as

$$\Delta\tau_{3d,2p} = \tau_{3d} - \tau_{2p} = (\tau_{\mathrm{SB2}} - \tau_{\mathrm{SB1}}) - \Delta\tau_{cc} - \Delta\tau_{\eta}, \quad (6)$$

where $\tau_{\mathrm{SB2}} - \tau_{\mathrm{SB1}}$ is the time delay from the phase difference between two SBs, $\Delta\tau_{cc}$ is the continuum-continuum transition time delay difference of two SBs, and $\Delta\tau_{\eta}$ is the scattering time delay difference of two SBs via the bound-continuum transition from $3d$ and $2p$ states. These three components are shown in Fig. 4(a) (blue line, red dashed line, and purple dot dashed line). The time delay between $3d$ and $2p$ states $\Delta\tau_{3d,2p}$ is less angular dependent and the average angular-dependent time delay is about -103 as.

Alternatively, one can directly obtain the time delay between the $3d$ and $2p$ states by tracing the wave function in real space. The trajectories of wave functions of $3d$ and $2p$ states are shown in Fig. 4(b) by tracing the maximum position of radial wave function of $3d$ and $2p$ during wave packet evolution. The maximum position of radial wave function $\mathrm{R_{nl}(r)}$ can be regarded as the center of the wave packets. At $t = 0$, the wave packets from $3d$ and $2p$ are located both around the atomic core. The wave packets' release from $3d$ and $2p$ subshells become spatially separated during the wavefunction propagating. It is obvious that the $3d$ wave packet appears earlier than the $2p$ wave packet for a given radius ($R = 25$ a.u.). Then the time delay of wave packets from those two states is almost unchanged. We obtain the time delay between the $3d$ wave packet and the $2p$ wave packet at about -95 as, as shown in Fig. 4(b). This is in good agreement with the angular-dependent average time delay between $3d$ and $2p$ states from the asymmetrical RABBITT geometry.

IV. CONCLUSION

In conclusion, we have studied the probing resonant photoionization delay between $3d$ and $2p$ states of the hydrogen atom via a different interference geometry of asymmetrical-photon transitions of using a fundamental laser pulse combined with its third harmonic to ionize the hydrogen atom. We obtain two SBs below the first ATI peak. These two SBs are the interference between the continuum-continuum transition from the first ATI and the direct ionization from the $3d$ and $2p$ bound states, respectively. By extracting the phase difference of two SBs, one is able to access to the intrinsic resonant time delay between $3d$ and $2p$ bound state, which is $\sim$103 as. By analyzing the wave function evolution, one can determine that it is valid to extract the time delay of atomic subshell in low-energy ATIs and SBs, which have strong coupling with the Coulomb potential and intermediate resonance states. The asymmetrical-photon transition interference method can be an alternative way to extract the intrinsic time delay of atomic subshells in the ultrafast dynamic process of the multiphoton ionization regime.

ACKNOWLEDGMENT

We acknowledge the support by the National Science Foundation of China (Grants No. 92050201, No. 11774013, and No. 11527901).

[1] M. Schultze, M. Fieb, N. Karpowicz, J. Gagnon, M. Korbman, M. Hofstetter, S. Neppl, A. L. Cavalieri, Y. Komnonos, Th. Mercouris *et al.*, Science **328**, 1658 (2010).

[2] K. Klünder, J. M. Dahlström, M. Gisselbrecht, T. Fordell, M. Swoboda, D. Guénot, P. Johnsson, J. Caillat, J. Mauritsson, A. Maquet, R. Taïeb, and A. L'Huillier, Phys. Rev. Lett. **106**, 143002 (2011).

[3] M. Huppert, I. Jordan, D. Baykusheva, A. von Conta, and H. J. Wörner, Phys. Rev. Lett. **117**, 093001 (2016).

[4] A. L. Cavalieri, N. Müller, Th. Uphues, V. S. Yakovlev, A. Baltuška, B. Horvath, B. Schmidt, L. Blümel, R. Holzwarth, S. Hendel *et al.*, Nature (London) **449**, 1029 (2007).

[5] Z. Tao, C. Chen, T. Szilvási, M. Keller, M. Mavrikakis, H. Kapteyn, and M. Murnane, Science **353**, 62 (2016).

[6] R. Kienberger, E. Goulielmakis, M. Uiberacker, A. Baltuska, V. Yakovlev, F. Bammer, A. Scrinzi, Th. Westerwalbesloh, U. Kleineberg, U. Heinzmann *et al.*, Nature (London) **427**, 817 (2004).

[7] J. Su, H. C. Ni, A. Jaron-Becker, and A. Becker, Phys. Rev. Lett. **113**, 263002 (2014).

[8] M. Sabbar, S. Heuser, R. Boge, M. Lucchini, T. Carette, E. Lindroth, L. Gallmann, C. Cirelli, and U. Keller, Phys. Rev. Lett. **115**, 133001 (2015).

[9] H. G. Muller, Appl. Phys. B **74**, s17 (2002).

[10] P. M. Paul, E. S. Toma, P. Breger, G. Mullot, F. Augé, Ph. Balcon, H. G. Muller, and P. Agostini, Science **292**, 1689 (2001).

[11] M. Han, P. Ge, Y. Shao, Q. Gong, and Y. Liu, Phys. Rev. Lett. **120**, 073202 (2018).

[12] P. Ge, M. Han, Y. Deng, Q. Gong, and Y. Liu, Phys. Rev. Lett. **122**, 013201 (2019).

[13] P. Ge, Y. Fang, Z. Guo, X. Ma, X. Yu, M. Han, C. Wu, Q. Gong, and Y. Liu, Phys. Rev. Lett. **126**, 223001 (2021).

[14] M. Han, P. Ge, J. Guo, Z. Guo, Y. Fang, X. Ma, X. Yu, Y. Deng, H. J. Worner, Q. Gong, and Y. Liu, Nat. Photonics **15**, 765 (2021).

[15] V. Véniard, R. Taïeb, and A. Maquet, Phys. Rev. A **54**, 721 (1996).

[16] G. Laurent, W. Cao, H. Li, Z. Wang, I. Ben-Itzhak, and C. L. Cocke, Phys. Rev. Lett. **109**, 083001 (2012).

[17] D. Guénot, K. Klünder, C. L. Arnold, D. Kroon, J. M. Dahlström, M. Miranda, T. Fordell, M. Gisselbrecht, P. Johnsson, J. Mauritsson, E. Lindroth, A. Maquet, R. Taieb, A. L'Huillier, and A. S. Kheifets, Phys. Rev. A **85**, 053424 (2012).

[18] M. Isinger, R. J. Squibb, D. Busto, S. Zhong, A. Harth, D. Kroon, S. Nandi, C. L. Arnold, M. Miranda, J. M. Dahlström, E. Lindroth, R. Feifel, M. Gisselbrecht, and A. L'Huillier, Science **358**, 893 (2017).

[19] M. Swoboda, T. Fordell, K. Klünder, J. M. Dahlström, M. Miranda, C. Buth, K. J. Schafer, J. Mauritsson, A. L'Huillier, and M. Gisselbrecht, Phys. Rev. Lett. **104**, 103003 (2010).

[20] A. Jiménez-Galán, L. Argenti, and F. Martín, Phys. Rev. Lett. **113**, 263001 (2014).

[21] A. Jiménez-Galán, F. Martin, and L. Argenti, Phys. Rev. A **93**, 023429 (2016).

[22] K. L. Ishikawa and K. Ueda, Phys. Rev. Lett. **108**, 033003 (2012).

[23] S. Haessler, B. Fabre, J. Higuet, J. Caillat, T. Ruchon, P. Breger, B. Carré, E. Constant, A. Maquet, E. Mével, P. Salieres, R. Taieb, and Y. Mairesse, Phys. Rev. A **80**, 011404(R) (2009).

[24] V. Gruson, L. Rarrean, A. Jiménez-Galan, F. Risoud, J. Caillat, A. Maquet, B. Carré, F. Lepetit, J. F. Hergott, T. Ruchon, L. Argenti, R. Taïeb, F. Martin, and P. Salières, Science **354**, 734 (2016).

[25] J. Caillat, A. Maquet, S. Haessler, B. Fabre, T. Ruchon, P. Salières, Y. Mairesse, and R. Taïeb, Phys. Rev. Lett. **106**, 093002 (2011).

[26] D. G. Arbó, S. Yoshida, E. Persson, K. I. Dimitriou, and J. Burgdörfer, Phys. Rev. Lett. **96**, 143003 (2006).

[27] A. S. Kheifets and A. W. Bray, Phys. Rev. A **103**, L011101 (2021).

[28] J. M. Dahlström, A. L'Huillier, and A. Maquet, J. Phys. B **45**, 183001 (2012).

[29] J. M. Dahlström, D. Guénot, K. Klünder, M. Gisselbrecht, J. Mauritsson, A. L'Huillier, A. Maquet, and R. Taïeb, Chem. Phys. **414**, 53 (2013).

[30] S. Heuser, Á. Jiménez Galán, C. Cirelli, C. Marante, M. Sabbar, R. Boge, M. Lucchini, L. Gallmann, I. Ivanov, A. S. Kheifets, J. M. Dahlström, E. Lindroth, L. Argenti, F. Martín, and U. Keller, Phys. Rev. A **94**, 063409 (2016).

[31] D. M. Villeneuve, P. Hockett, M. J. J. Vrakking, and H. Niikura, Science **356**, 1150 (2017).

[32] A. W. Bray, F. Naseem, and A. S. Kheifets, Phys. Rev. A **97**, 063404 (2018).
[33] I. A. Ivanov and A. S. Kheifets, Phys. Rev. A **96**, 013408 (2017).
[34] L. J. Zipp, A. Natan, and P. H. Bucksbaum, Optica **1**, 361 (2014).
[35] P. P. Ge, M. Han, M-M. Liu, Q. H. Gong, and Y. Q. Liu, Phys. Rev. A **98**, 013409 (2018).
[36] C. Cirelli, C. Marante, S. Heuser, C. L. M. Petersson, A. Jiménez, L. Argenti, S. Y. Zhong, D. Busto, M. Isinger *et al.*, Nat. Commun. **9**, 955 (2018).
[37] P. Hockett, J. Phys. B: At. Mol. Opt. Phys. **50**, 154002 (2017).
[38] D. Busto, J. Vinbladh, S. Y. Zhong, M. Isinger, S. Nandi, S. Maclot, P. Johnsson, M. Gisselbrecht, A. L'Huillier, E. Lindroth, and J. M. Dahlström, Phys. Rev. Lett. **123**, 133201 (2019).
[39] A. Harth, N. Douguet, K. Bartschat, R. Moshammer, and T. Pfeifer, Phys. Rev. A **99**, 023410 (2019).
[40] J. Fuchs, N. Douguet, S. Donsa, F. Martin, J. Burgdörfer, L. Argenti, L. Cattaneo, and U. Keller, Optica **7**, 154 (2020).
[41] P. K. Maroju, C. Grazioli, M. D. Fraia, M. Moioli, D. Ertel, H. Ahmadi, O. Plekan, P. Finetti, E. Allaria, L. Giannessi *et al.*, Nature (London) **578**, 386 (2020).